Versatile and high temperature spectroscopic cell for *operando* fluorescence and transmission X-ray absorption spectroscopic studies of heterogeneous catalysts

Daniel Eggart,[1] Anna Zimina,[2] Gülperi Cavusoglu,[1] Maria Casapu,[1] Dmitry E. Doronkin,[1,2] Kirill A. Lomachenko,[3] Jan-Dierk Grunwaldt[1,2,a]

[1] Institute for Chemical Technology and Polymer Chemistry (ITCP), Karlsruhe Institute of Technology (KIT), Engesserstraße 20, 76131 Karlsruhe, Germany

[2] Institute of Catalysis Research and Technology (IKFT), Karlsruhe Institute of Technology (KIT), Hermann-von-Helmholtz-Platz 1, 76344 Eggenstein-Leopoldshafen, Germany

[3] European Synchrotron Radiation Facility, 71 Avenue des Martyrs, CS 40220, 38043 Grenoble Cedex 9, France

[a] Author to whom correspondence should be addressed: grunwaldt@kit.edu

A modular high-temperature cell consisting of a plug-flow microreactor with fixed catalyst bed and long heating zone has been established for *operando* X-ray absorption/fluorescence spectroscopic and diffraction studies. The functionality of the cell is demonstrated for two important areas: emission control using a 2 wt.% Pd/Al_2O_3 acting as three-way catalyst and direct conversion of methane to olefins and aromatics on a 0.5 % Fe/SiO_2 catalyst. The performance has been determined by on-line infrared spectroscopy and mass spectrometry, respectively. In addition, the cell can be combined with optical spectroscopy, such as Raman spectroscopy. The catalyst, present as powdered/sieved samples, can be measured under reaction conditions at temperatures of up to 1050 °C. Another key aspect is a long isothermal heating zone with small temperature gradient (< 3 °C/mm at 1000 °C without reaction) including an inert zone for pre-heating of the reactant gas. Due to the small size of the microreactor and the heating system including a water cooling system, heating/cooling rates of up to 100 °C/min can be achieved. Moreover, due to the compact design and the autonomous control system, the high temperature *operando* setup fits to the space at the majority of synchrotron beamlines. In many cases the element of interest in the catalysts is low requiring X-ray absorption spectroscopy measurements in the fluorescence measurement mode. Hence, the microreactor was designed to fit such needs as well. More specifically, the case of Fe-containing catalysts was particularly considered by using iron-free materials for the reactor housing.

I. INTRODUCTION

Understanding heterogeneous catalysts in terms of interaction between the active sites and the support, activation and deactivation pathways as well as regeneration conditions is key for improved design and development of highly active and stable catalysts.[1-5] These questions are best answered with characterization methods that allow measurement of catalysts under reaction conditions.[6, 7] In this regard, X-ray absorption spectroscopy (XAS) is a highly suitable method for *operando* investigation of heterogeneous catalysts under realistic conditions due to the high penetration depth of the high-energy X-rays.[8-12] Variations in oxidation states and local geometry of active sites can be derived from the X-ray absorption near edge structure (XANES) data whereas detailed information on the coordination environment, such as a type of neighbors, interatomic distances and coordination numbers, can be obtained by analysis of the extended X-ray absorption fine structure (EXAFS) data.[11, 12] For example, a reduction protocol to vary the size and dispersion of Pt nanoparticles on CeO_2 in order to tune the catalytic activity for total oxidation reactions was proposed with the help of *operando* XAS.[13] Moreover, XAS can be easily combined with other *operando* methods in order to acquire complementary information about the crystalline structure of support or nature of the adsorbed species, for instance.[9, 14] This approach was for example applied to study the hydrocarbon activation step during selective oxidation of propene by bismuth molybdates with combining *operando* XAS and X-ray diffraction (XRD)/Raman spectroscopy, and led to a holistic understanding of the multicomponent catalyst redox behavior influencing the catalytic performance.[15]

During the last decades, a wide array of XAS cells has been developed to measure catalyst powders or pellets at elevated temperatures (of > 750 °C) under reaction gas atmosphere.[12, 16-22] In each of these designs, the best compromise between optimal performance in spectroscopy and catalysis must be found.[10, 23] To overcome pore diffusion problems occurring whilst measuring pellets, a commonly used plug-flow setup features sieved catalysts placed between two quartz wool plugs in a quartz capillary heated by a gas blower.[23] This concept was firstly introduced by Clausen *et al.*[24] and Sankar *et al.*[25]. It has been further developed by Grunwaldt *et al.*[23] and allows the combination of XAS with scattering techniques (XRD; small angle X-ray scattering, SAXS) and optical spectroscopies, for instance UV-Vis, Raman spectroscopy and IR thermography.[26] In our experience, achieving temperatures above 800 °C and avoiding temperature gradients over the catalytic bed is challenging with a capillary microreactor heated by a gas stream blower. Gradients at temperatures below 700 °C have been circumvented using special housings. To overcome these difficulties, several alternatives have been more recently proposed by various research groups. Higher temperatures of up to 1000 °C can be reached with a cell developed by Aguilar-Tapia *et al*.[27] In this setup, the sample is placed within a glassy carbon tube heated by surrounding molybdenum wires where He atmosphere protects both from oxidation. In general, glassy carbon has a higher transmittance of X-rays than quartz but is more easily corroded by oxidative gas atmospheres, limiting the feasible reaction gas atmospheres. An alternative plug-flow microreactor firstly introduced by Chupas *et al.*[28] and then improved by Figueroa *et al.*[29] focuses IR radiation of two Kanthal® A-1 heating wire coils with a circular aluminum shield around a quartz capillary. Thereby, a low axial temperature gradient along the catalyst bed at a maximum operating temperature of about 900 °C has been reported.[29] The relatively large front openings allow measurement of X-ray absorption, fluorescence and XRD but have to be covered by Kapton tape to reduce temperature fluctuations by air circulation.[29] Andrieux *et al.* introduced an advanced cell design for *operando* XRD measurements with the sample placed in a sapphire tube

heated by Fe-Ni-Cr Kanthal® wires up to 1000 °C. The sample can be rotated by a goniometer and the unique gas dosing system allows pressure ranges of 10^{-3} mbar - 200 bar. [30]

In addition to providing the desired reaction conditions, i.e. high temperature, low temperature gradients along the catalyst bed and plug-flow geometry, an advanced *operando* cell for XAS studies should also be applicable to study catalysts with low content of the active species. Such metal-based catalysts are often applied for relevant industrial processes. For instance, Fe single-sites supported on silica (< 1 wt. % Fe loading) gained increasing attention due to their high activity in the direct conversion of methane to ethylene and aromatics at temperatures above 950 °C. [31-35] However, their structure under operating conditions is strongly discussed and X-ray absorption spectroscopy (XAS) would be an ideal technique to investigate this. A similar situation is encountered in the case of emission control catalysts, which typically contain small amounts of Pt, Pd and/or Rh supported on γ-Al_2O_3 and $Ce_xZr_yO_z$. [36] Despite they have been exploited since decades in real applications, detailed structure-activity relationships still need to be derived in order to improve their activity and comply with stricter emission regulations. However, measuring *operando* XAS on such catalysts is challenging because of the broad temperature window (up to 1000°C) and highly absorbing carrier components, as for example demonstrated for Pt-CeO_2-based catalysts. [13, 37] Analogously, *operando* XAS investigations on samples with low loading of iron is even more difficult, as iron in stainless steel or aluminum from the sample surroundings tends to interfere with the fluorescence signal of the measured sample. None of the so far introduced setups allows XAS measurements in fluorescence mode of samples with low iron content of less than 1 wt.% at elevated reaction temperatures of up to 1000 °C. Hence, here we present an *operando* plug-flow microreactor specifically designed to sustain high temperatures of up to 1050 °C for several days, low heat capacity for rapid heating/cooling, long isothermal zone and, finally, to reduce Fe X-ray fluorescence noise by minimizing the Fe content in the reactor housing and shielding the X-ray beam from iron containing parts. The aim is to use modular components to allow the combination of different *operando* methods as well as a user-friendly assembly for switching between the measurement methods. The reactor design targeted not only a small size but also a manufacturing at a rather low cost with simple heating system compared to e.g. rather cost-intensive and complex high temperature gas blowers systems.

II. DESCRIPTION OF THE SPECTROSCOPIC *OPERANDO* CELL

A. *Operando* cell with fixed-bed microreactor

The 3D layout of a new plug-flow reactor, inspired by the earlier designs described in the introduction and particularly by the setup in work [29] , is shown in Fig. 1. The basic principle is the use of heating wires for reactor heating, a quartz or similar capillary as a plug flow reactor and adjustment of the sample in the middle by a linear motion guide. During the design of the cell, special attention was paid to the modular components which were optimized for an easy-to-handle configuration of the setup whilst allowing *operando* X-ray transmission, fluorescence and diffraction measurements. Several iron-free materials were evaluated for the oven housing with respect to their melting point, IR reflectivity and ease of machining. Thereby, copper was chosen due to its high IR reflectivity of about 98 % [38] and melting point of 1,083 °C [39]. Interchangeable shielding windows allow not only user-friendly switching, but also combination of the characterization methods. For fluorescence measurements, the front window is closed

and the side windows can vary in diameter depending on the detector size (Fig. 1 a). High-energy diffraction measurements are possible with the front window fully open giving a 2θ range of 8.5 ° (Fig. 1 c). Furthermore, X-ray spectroscopy can be coupled with optical spectroscopy such as Raman spectroscopy. Filling of the plug-flow micro reactor, the heating/cooling system and the linear motion guide are described in the following. Note that the whole assembly is mounted on an x,y,z-Table or a hexapod system to adjust it in the synchrotron beam and has been tested at various beamlines (e.g. P65 at DESY [40] and CAT-ACT at KIT [41]).

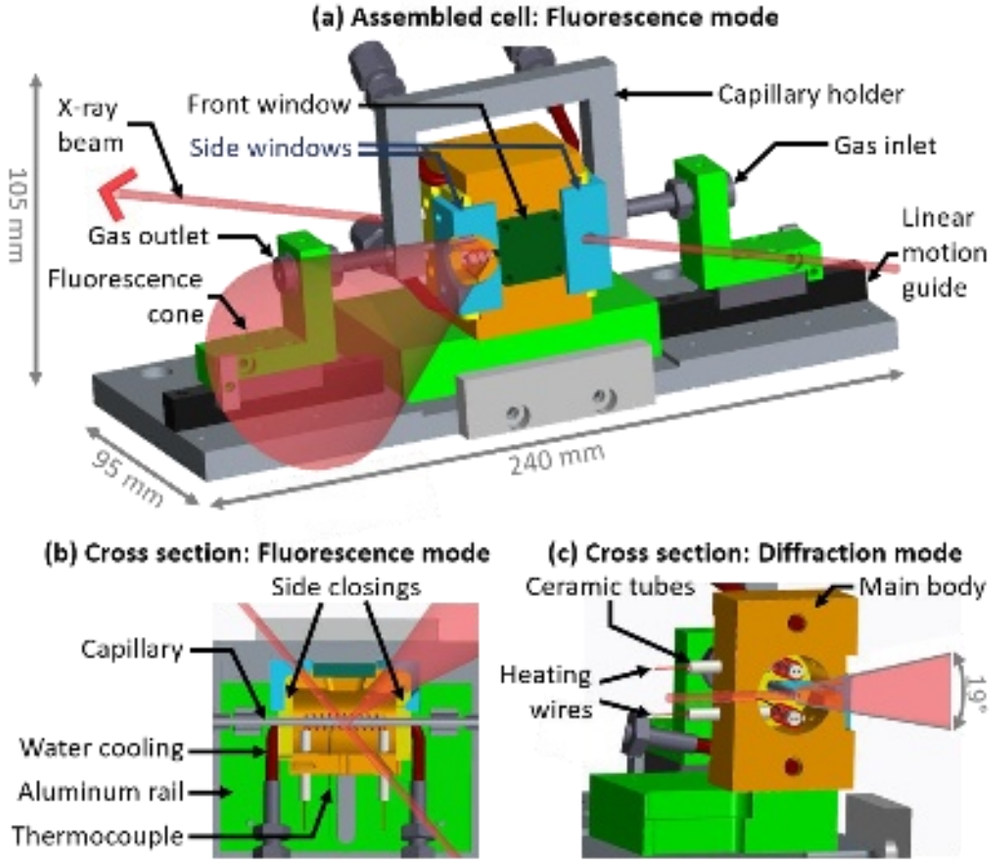

Fig. 1: 3D layout of the (a) fully assembled microreactor setup in XAS fluorescence mode (side windows open (cyan), front shielding window (green), capillary as key for the fixed bed reactor and capillary holder, the oven body (orange) with heating wires and water cooling system (red) mounted on a rail for alignment) and (b) cross section view thereof; (c) cross section view of the microreactor in diffraction mode (side windows closed, front window open).

For preparation of the microreactor, the sieved catalyst material (grain size typically 50-250 µm) is placed between two quartz wool plugs in a quartz capillary (0.5-3 mm OD and 10-40 µm wall thickness, WJM-Glas Müller GmbH). The microreactor is then sealed airtight in an aluminum capillary holder (Fig. 1 a) with high-temperature epoxy glue (LOCTITE® EA 3450, Henkel), similarly to the one described in reference [42]. The setup can be used at pressures of at least 20 bar. [43] The capillary diameter is selected depending on the X-ray transmission through the sample and can also be used to adjust the gas hourly space velocity (GHSV). The wall thickness depends on the incident X-ray energy as well as the intended pressure range of the reaction gas. The capillary holder is mounted on a linear motion guide (THK GmbH, SRS-G) enabling precise positioning of the catalyst bed in the middle of the reactor (Fig. 1 a). Through Swagelok® fittings

attached to the capillary holder the connection to a gas dosing and to a gas analysis system are possible. Additionally, several capillary holders allow for prearrangement of the capillaries and thereby accelerated exchange of the samples during beamtime. Once the capillary holder is fixed, the main reactor body can be slid on an aluminum rail over the capillary (Fig. 1 b). The rail is fixed on an aluminum plate which can be positioned on any movable stage available at the beamline for the alignment of the cell to the beam. The fully assembled cell is relatively small (240 x 95 x 105 mm; length x width x height), weighs about 2 kg and therefore fits to the space available for the sample environment at the majority of beamlines. An image of the working reactor at 975 °C can be seen in Fig. 2. Additional images and drawings of the microreactor are given in Fig. S 1 – 4.

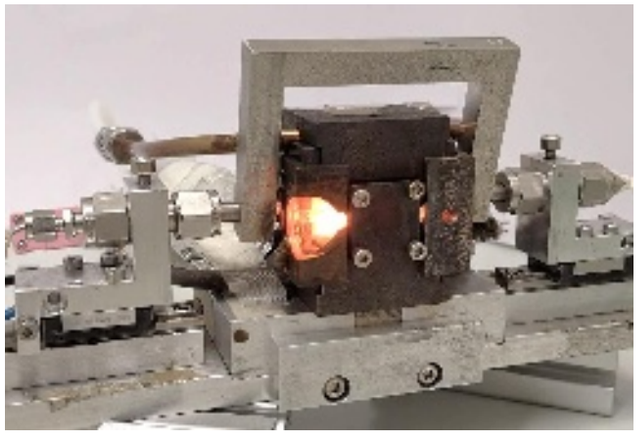

Fig. 2: Image of the microreactor at 975 °C reaction temperature with the windows arranged for XAS measurements in fluorescence mode and the side window closed with Kapton tape.

B. Heating system

The low-weight heating/cooling system is a key part of the *in situ* microreactor. For this purpose, heating wires (Kanthal® A1, 1.0 mm diameter, EWWK GmbH, NT0019-H) are coiled around a ceramic tube (4 mm OD x 28mm long, Aliaxis Deutschland GmbH, F143-11040-00028) and isolated from the main oven body by ceramic tubes (Aliaxis Deutschland GmbH, F122-11004-00025) (Fig. 1 c). 16 windings equally distanced for each coil are connected in parallel and give an average resistance of 1.3 Ω at room temperature. Instead of using 0.5 mm diameter resistive wire as reported by Chupas *et al.* [28], a thicker wire of 1.0 mm diameter was used prolonging its lifetime at elevated operation temperatures. In order to circumvent gas conversion by thermocouples, the thermocouple (N-type, 0.5 mm diameter, TC Mess- und Regeltechnik GmbH, 406-601) is positioned outside the capillary inside the oven closely to the center of the catalyst bed (Fig. 1 b). The thermocouple is fixed to the reactor main body with a screw and accidental removal is prevented by a clamp fixed to the slide rail. An additional thermocouple can be put inside the capillary in direct contact with the catalyst bed through a ferrule in a Swagelok® Tee piece for the direct temperature calibration. The resistive wires of two heating coils (above and below the microreactor) are connected in series to a direct current supply (Delta Elektronika, SM 70-AR-24-P258, max. 0 – 35 V / 0 – 24 A / 800 W) and the temperature is regulated by a Eurotherm 2416 controller (heating output between 0 and 5 V). The capillary is positioned in the center of the main body's cavity between the two coils and is therefore homogeneously heated by the focused IR radiation. Sudden temperature changes are avoided through

minimization of air circulation by closing the window's apertures with Kapton tape. Thereby, a maximum temperature in the capillary of 1050 °C can be reached and maintained for several days. The temperature of the cell's outer body does not exceed 100 °C below 800 °C operating temperature due to passive air cooling (convection). Above 800 °C operating temperature, water cooling is necessary to prevent possible overheating of the beamline components (e.g. the piezo-motors of a hexapod positioning system installed at the CAT-ACT beamline at KIT's synchrotron radiation source) and of the Be window of the fluorescence detector. With the water cooling at 23°C, heating and cooling rates of up to 100 °C/min can be realized.

C. Temperature profile in the heating zone

The reaction rates over catalysts are strongly dependent on the temperature. Hence, a stable and homogeneous temperature profile along the catalyst bed is required for *operando* spectroscopic experiments. In addition, the overall X-ray absorption and edge jump of the element of interest needs to be adjusted. Hence, depending on the penetration depth of the X-rays and the concentration of the investigated element, capillaries of different diameters were used. Usually, diameters of 1-2 mm have given the best results for *operando* transmission XAS measurements. Considering the use of a sieve fraction of 100 µm, adjustment of the gas flow vs. catalyst bed volume/mass thereby results in a catalyst bed length of 5-10 mm. For the *operando* XAS measurements reported in this study, the applied catalyst bed length was 6 mm for capillaries of 1.5 mm diameter. Temperature profiles were recorded by pulling a thermocouple (0.25 mm diameter) fixed on a movable stage out of a capillary (1.5 mm O.D.) with the catalyst bed fixed between two quartz wool plugs. Temperature distributions at a 400 °C and 1000 °C setpoint with the water cooling system in use along a 40 mm catalyst bed of 2.5 % Pt/CeO_2 (100-200 µm sieve fraction) at 5 and 50 mL/min He flow are shown in Fig. 3. The average axial temperature gradient varies within the area of interest (over 6 mm bed length centered in the microreactor, Fig. 3) depending on the gas flow with about 2.2 °C/mm (5 mL/min) and 2.7 °C/mm (50 mL/min) at 1000 °C. At 400 °C, the average axial temperature gradient for 6 mm bed length alters from 1.5 °C/mm (5 mL/min) to 1.8 °C/mm (50 mL/min). We conclude that the temperature homogeneity is very good in this microreactor, we expect that mostly the applied gas flow and reaction enthalpy (exothermic/endothermic reaction) have a more pronounced effect on the temperature gradient and should be e.g. determined by an IR camera. [44, 45] Compared to the design by Figueroa *et al.* [29], using aluminum instead of copper yields a lower axial temperature gradient of ≈ 0.13 °C/mm at temperatures above 670 °C due to a lower heat loss on the basis of lower heat conductivity of Al (237 W/m·K) than Cu (401 W/m·K). [46] Some reduction of axial temperature gradient of the proposed cell could be achieved by heating of the gas inlet pipes. Furthermore, addition of an insulating ceramic parts with apertures for the heating wires and X-ray windows would further reduce the heat loss. Nevertheless, in comparison to microreactor setups with commercial gas blowers, the temperature is more homogeneous over a larger section of the microreactor. In addition, in the present setup, the reactant gas can be sufficiently pre-heated in the zone before entering the fixed bed containing the catalyst. Challenges with this reactor remain with respect to the brittleness of the capillary, especially if only 10 µm thin quartz capillaries need to be used and that in case of too long beds a plugging and thus a too high-pressure drop may occur. The aspect of brittleness is minimized by fixing the capillaries to the capillary holder with epoxy glue (similar as in reference [42]). However, after prolonged heating (> 10 h) with temperatures exceeding 900 °C, the epoxy glue tends to get very rigid and the capillary can only be removed from the capillary holder by breaking it off (see ESI for more detailed discussion). Since

the temperature regulation is highly sensitive to the position of the thermocouple, the temperature should be recalibrated after every assembly of the setup.

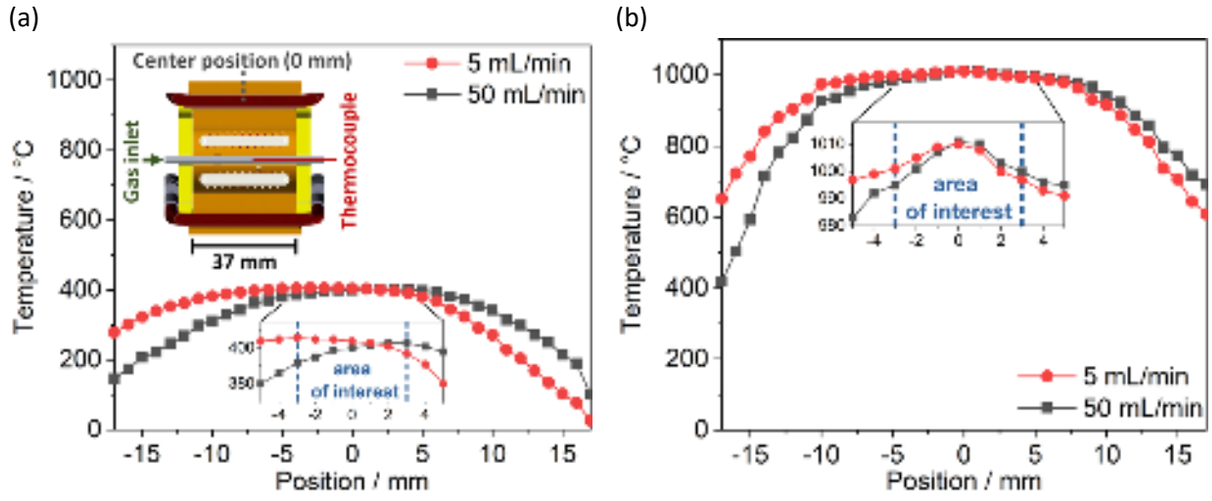

Fig. 3: Temperature profile at a setpoint of (a) 400 °C and (b) 1000 °C along a 40 mm catalyst bed filled with 2.5 wt.% Pt/CeO_2, 100-200 µm sieve fraction, quartz capillary 1.5 mm OD and 20 µm wall thickness at 5 and 50 mL/min He flow; center of the microreactor at 0 mm and gas inlet at about -25 mm position; area of interest for determination of temperature gradient from -3 to +3 mm; a) cross section inset of the microreactor.

D. Fluorescence XAS measurements of samples with iron loading below 1 wt.%

One of the further main objectives for this setup is to enable the XAS measurements in fluorescence mode of samples with low iron loading at temperatures of up to 1000 °C without interference signals from surrounding Fe-containing environment. For this purpose, the housing of the oven has been made of iron-free Cu-ETP (EDX measurement cf. Fig. S 5, XRF measurement cf. Fig. S 6) instead of Aluminum. [29] At the same time, the N-type thermocouple sheath is made of iron-free Nicrotherm D™ and finally, the iron containing Kanthal® A1 heating wire (iron-chromium-aluminum alloy [47]) is protected from X-rays through the arrangement of the windows. The entrance window of the X-ray fluorescence detector can be shielded with iron-free copper sheets instead of aluminum foil to reduce Fe fluorescence background signals from the surrounding equipment at the beamline. With the proposed cell design, it was possible to measure Fe K_α X-ray fluorescence of a 0.04 % Fe/SiO_2 sample with 90 % of the fluorescence signal originating from the sample (cf. Fig. S 7). The residual X-ray fluorescence Fe background signals most likely originated from surrounding beamline equipment and not from the microreactor setup (cf. Fig. S 7). Therefore, the proposed arrangement gave the best compromise between low Fe X-ray fluorescence noise and optimal temperature profile along the catalyst bed.

III. APPLICATION: XANES/EXAFS INVESTIGATIONS

A. Experimental

XAS measurements were conducted at the P65 beamline of the PETRA III synchrotron radiation source (DESY, Hamburg) in transmission mode using ionization chambers for Pd K-edge (24.350 keV) and combining transmission/fluorescence mode using an additional 7 pixel HPGe detector (Canberra GmbH)

for Fe K-edge (7.112 keV). [40] The source of X-rays is an 11 period undulator and Higher harmonics were rejected by a pair of plane mirrors (Si for Fe K-edge and Pt-coated Si for Pd K-edge) installed in front of the monochromator. The energy of X-ray photons was further selected by a Si(111) for Fe K-edge and Si(311) for Pd K-edge double-crystal monochromator and the beam size was set with slits to 1.0 x 0.2 mm^2. XANES spectra were recorded in rapid continuously scanning mode and EXAFS spectra were acquired in step scanning mode. The spectra were processed using the ATHENA program from the Demeter software package. [48] The catalyst powder (sieved fraction size= 100-200 µm) was loaded in a quartz capillary (100 mm length, outer diameter = 1.5 mm, wall thickness= 0.02 mm) and fixed between two quartz wool plugs. Gases were dosed with the mass flow controllers (Bronkhorst) and analyzed with either the mass spectrometer (MS, Pfeiffer Vacuum, OmniStar GSD 320 T) or the online Fourier-transform infrared spectrometer (FTIR, MKS, Multigas MG2030). The exhaust gas lines were heated to 150 °C.

The 2 wt.% Pd/Al_2O_3 three-way catalyst was prepared by incipient wetness impregnation method using palladium acetylacetonate (STREAM Chemicals, 99%) as precursor and commercial γ-Al_2O_3 (SASOL Germany GmbH) as support material. [49] After impregnation, the sample was calcined at 500 °C for 2 h in static air. The catalytic activity was evaluated by feeding a gas mixture of 3000 ppm CO, 1000 ppm NO, 1000 ppm C_3H_6, 5400 ppm O_2, 3% H_2O and He in balance (stoichiometric three-way reaction condition, λ≈1) with a total flow of 50 mL/min at atmospheric pressure (GHSV = 60,000 h^{-1}). The light-off/light-out experiments (heating-/cooling-cycle) were performed between 40 and 800 °C with a temperature ramp of 10 °C/min.

The 0.5 % Fe/SiO_2 catalyst was prepared by flame spray pyrolysis from a 1.0 mol/L solution of Iron(III) acetylacetonate (Acros Organics, 99%) and Tetraethyl orthosilicate (Alfa Aesar, 99.9%) in xylene (VWR chemicals). [50] For *operando* studies, either He, 90% CH_4/He or 20% O_2/He at atmospheric pressure with a total gas flow of 5 mL/min were dosed (GHSV = 29,000 h^{-1}).

The chemical contents of catalyst samples were determined with a triple determination via inductively coupled plasma optical emission spectroscopy (ICP-OES) on an iCAP 7600 Duo spectrometer (Thermo Fischer Scientific).

B. Pd/Al_2O_3 three-way catalyst

As a first case study for demonstrating the use of the new setup in typical *operando* investigations in heterogeneous catalysis, *operando* XAS was conducted at the Pd K-edge (24,350 eV) for a Pd/Al_2O_3 catalyst during transient light-off/light-out measurements between room temperature and 800°C under usual reaction conditions of a three-way catalyst (TWC). TWCs are widely applied for emission control of gasoline powered vehicles, to simultaneously convert CO, HC and NO_x into CO_2, H_2O and N_2. The active components in TWCs are precious metals such as Pt, Pd or Rh and the support materials are mostly γ-Al_2O_3, CeO_2 and ceria-based composite oxides. [36] Despite the extensive application of TWCs, the reaction mechanism, the structural variation of the noble metal sites and the noble metal – support are still debated in literature. [51, 52] Hence, applying *operando* methods like XAS to elucidate the catalyst behavior under reaction conditions is highly relevant. In the present study EXAFS spectra were recorded at room temperature in static air before exposure to reaction mixture to characterize the initial state of the catalyst. Afterwards, the cell was heated from room temperature to 800 °C with a temperature ramp of

10 °C/min and cooled down with the same temperature ramp. During the light-off/light-out cycle XANES spectra were recorded under stoichiometric reaction condition, which allowed to monitor the change in the metal oxidation state. Pd K-edge XANES and EXAFS spectra as well as the Fourier transformed EXAFS spectra recorded at room temperature at different reaction conditions before and after catalytic tests are shown in Fig. 4. The XANES and EXAFS spectrum of the as-prepared sample in static air and in reaction mixture at room temperature resemble that of PdO reference. Accordingly, the corresponding Fourier transformed EXAFS spectra (Fig. 4 c) shows two main backscattering peaks at around 1.5 Å and 3.0 Å, associated to the first (Pd–O) and second (Pd–Pd) coordination shells, respectively, of a PdO-like phase. After the light-off/light-out cycle, the collected XANES and EXAFS data mainly indicated the formation of metallic Pd particles. The corresponding Fourier transformed (FT) EXAFS data showed a main backscattering around 2.5 Å, which was assigned to the first Pd–Pd coordination shell of metallic Pd.

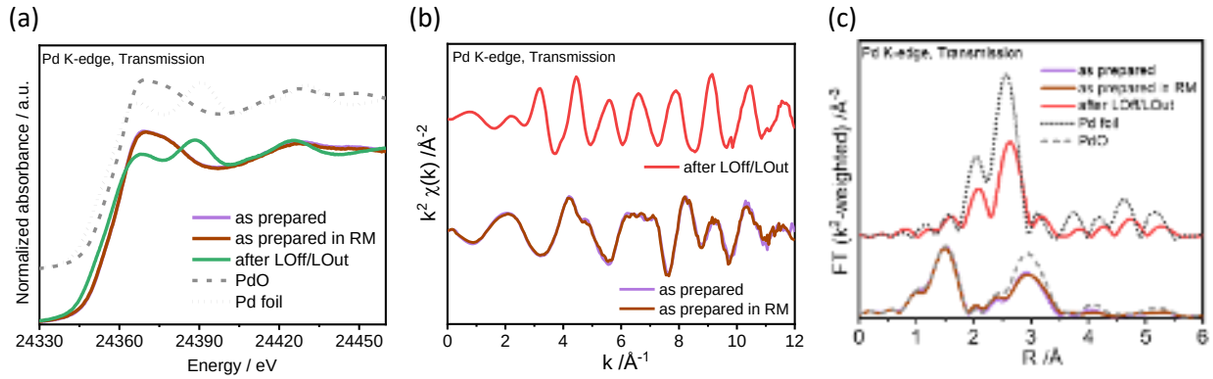

Fig. 4: Pd K-edge XANES spectra (a) and EXAFS refinement data in (b) k- and (c) R-space (not corrected for phase shift) before and after light-off/light-out cycle recorded at room temperature under state steady conditions after following *operando* treatment: as prepared, as prepared in reaction gas mixture and after light-off/light-out.

Fig. 5 depicts the *operando* XANES spectra at the Pd K-edge as recorded during the light-off/light-out cycle. The results show no significant change of the XANES profile during light-off (Fig. 5 a) up to around 160 °C, where CO conversion started (Fig. 6). Above this temperature a relatively sharp decrease of the white line was observed, indicating the reduction of Pd particles. A further increase of the reaction temperature to 800 °C led to complete Pd reduction, in line with similar studies on Pd-based TWCs. [53, 54] After reaching 800 °C the sample was cooled to room temperature and hardly any changes were observed in the XANES region of Pd K-edge (Fig 5 b).

Simultaneously to monitoring of the catalyst structure, the TWC activity was measured by an online FTIR analyzer. The CO, C_3H_6 and NO conversion recorded during the light-off/light-out cycle of 2 wt.% Pd/Al_2O_3 is shown in Fig. 6. The results indicate an earlier oxidation onset for CO with a temperature of 50% conversion (T_{50}) at 170 °C. Around this temperature Pd species were already partially reduced (Fig. 5a). Only when CO is considerably oxidized (about 50% conversion) and Pd is almost completely reduced, C_3H_6 starts to convert and is immediately followed by NO reduction (T_{50} at 240 and 250 °C, respectively). These activity trends are in line with previous studies on similar catalysts.

During the light-out activity test (Fig. 5b), an inverse hysteresis in CO conversion is observed with an increase of T_{50} by about 90 °C. The T_{50} variation could be due to the slight sintering and formation of

metallic Pd particles during exposure to high temperatures. In contrast, a smaller inverse hysteresis is observed during the light-out of NO and C_3H_6 conversion, which show a T_{50} shifted by 20 °C towards the higher temperature. The smaller variation could be caused by the lower sensitivity of the NO reduction and C_3H_6 oxidation to the change in Pd structure, since distinct effects are known to appear for different reactions catalyzed by noble metal emission control catalysts. [55, 56]

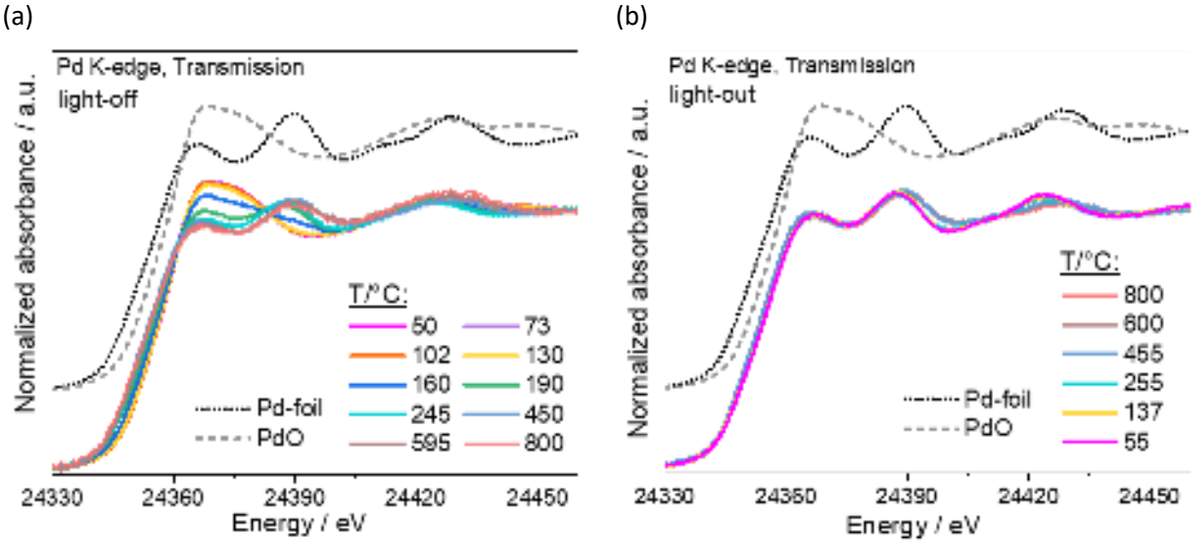

Fig. 5: Normalized Pd K-edge XANES spectra for the 2 wt.% Pd/Al_2O_3 catalyst and for PdO and Pd foil as references recorded during (a) light-off and (b) light-out under stoichiometric three-way reaction condition, λ≈1 (3000 ppm CO, 1000 ppm NO, 1000 ppm C_3H_6, 5400 ppm O_2, 3% H_2O and He in balance).

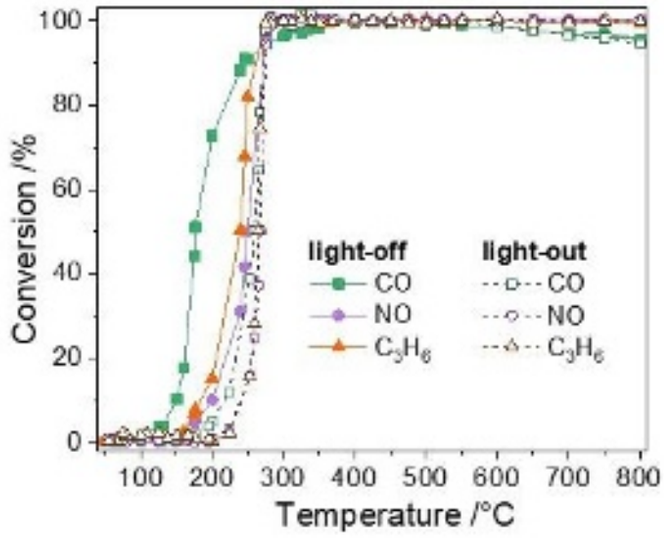

Fig. 6: Conversion of CO, NO and C_3H_6 during light-off/light-out under stoichiometric three-way reaction condition recorded via FTIR with the microreactor in parallel to the *operando* XAS measurements, λ≈1 (3000 ppm CO, 1000 ppm NO, 1000 ppm C_3H_6, 5400 ppm O_2, 3% H_2O and He in balance), measured by on-line FTIR.

C. Fe/SiO_2 for direct conversion of methane to olefins and aromatics

As a second case study, 0.5 % Fe/SiO_2 catalyst for direct non-oxidative conversion of methane was measured in fluorescence and transmission modes at the Fe K-edge (7,112 eV). Recently discovered resources of methane increased the attention for processes which can directly convert methane into fuels and high value-added chemicals such as ethylene and aromatics. [57] A newly proposed route, tackling remaining issues of low yield and stability, typically requires temperatures above 950 °C and low iron loading (< 1 wt.%) on SiO_2 supports. [31-35] Hence, this application allows to demonstrate the microreactor performance during *operando* XAS of catalysts with low loading of iron and high reaction temperatures (> 900 °C). The applied *operando* measurement procedure with heating to 975 °C, reaction gas atmosphere in CH_4/He, switching to 90% O_2/He and cooling to room temperature as well as the recorded MS signals are reported in Fig. 7. A linear heating ramp of 30°C/min were conducted. As soon as the gas atmosphere is switched to methane, ethylene (m/z = 27) and aromatics (m/z = 78) are detected by the MS as reaction products. Additional MS signals of hydrocarbon product fragments are shown in Fig. S 8.

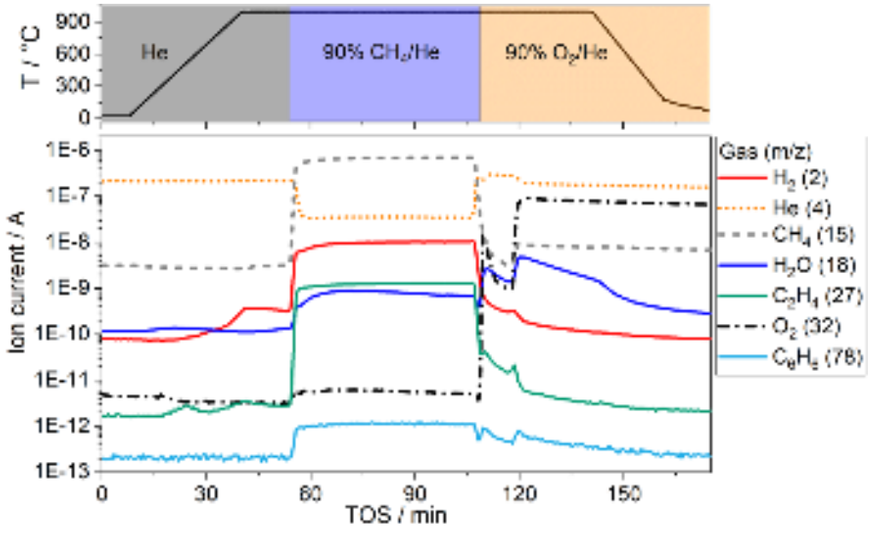

Fig. 7: Procedure of the *operando* experiment (top) and mass spectrometer signals (bottom) for 0.5 % Fe/SiO_2 for heating up in He with 30 °C/min to 975 °C, 50 min reaction in 90% CH_4/He and oxidation in 20% O_2/He and cooling down to 40 °C with 40 °C/min.

During heating up in He, Fe undergoes a slight auto-reduction that has been already reported in literature (cf. Fig. S 9). [58] The XANES fluorescence measurements at different reaction conditions are shown in Fig. 8: At 975 °C in He atmosphere Fe is in a highly reduced state, which merely changes during CH_4 conversion; the introduction of O_2 leads to a slight oxidation of Fe (Fig. 8 a, c). Simultaneous recording of transmission data during the reaction confirmed these findings and are not limited by the cell but rather by the low concentration of iron in the sample. (Fig. 8 b, d) In fact, small differences as compared to the CH_4/He fluorescence data were observed in the derivative of the transmitted XANES spectra, which resulted from a lower signal-to-noise ratio of the transmission measurement due to the low Fe loading. Hence, for future experiments with the similar sample parameters, the fluorescence mode seems to be more appropriate. Furthermore, additional in-depth studies are necessary to evaluate the nature of the active sites during methane conversion to higher alkenes and aromatics. This proof of concept demonstrates that the cell now opens up experiments at elevated temperatures for case studies which are challenging even at lower

temperatures, as e.g. discussed for low-concentrated Fe-based catalysts during selective catalytic reduction of NO_x by ammonia in ref. [59]

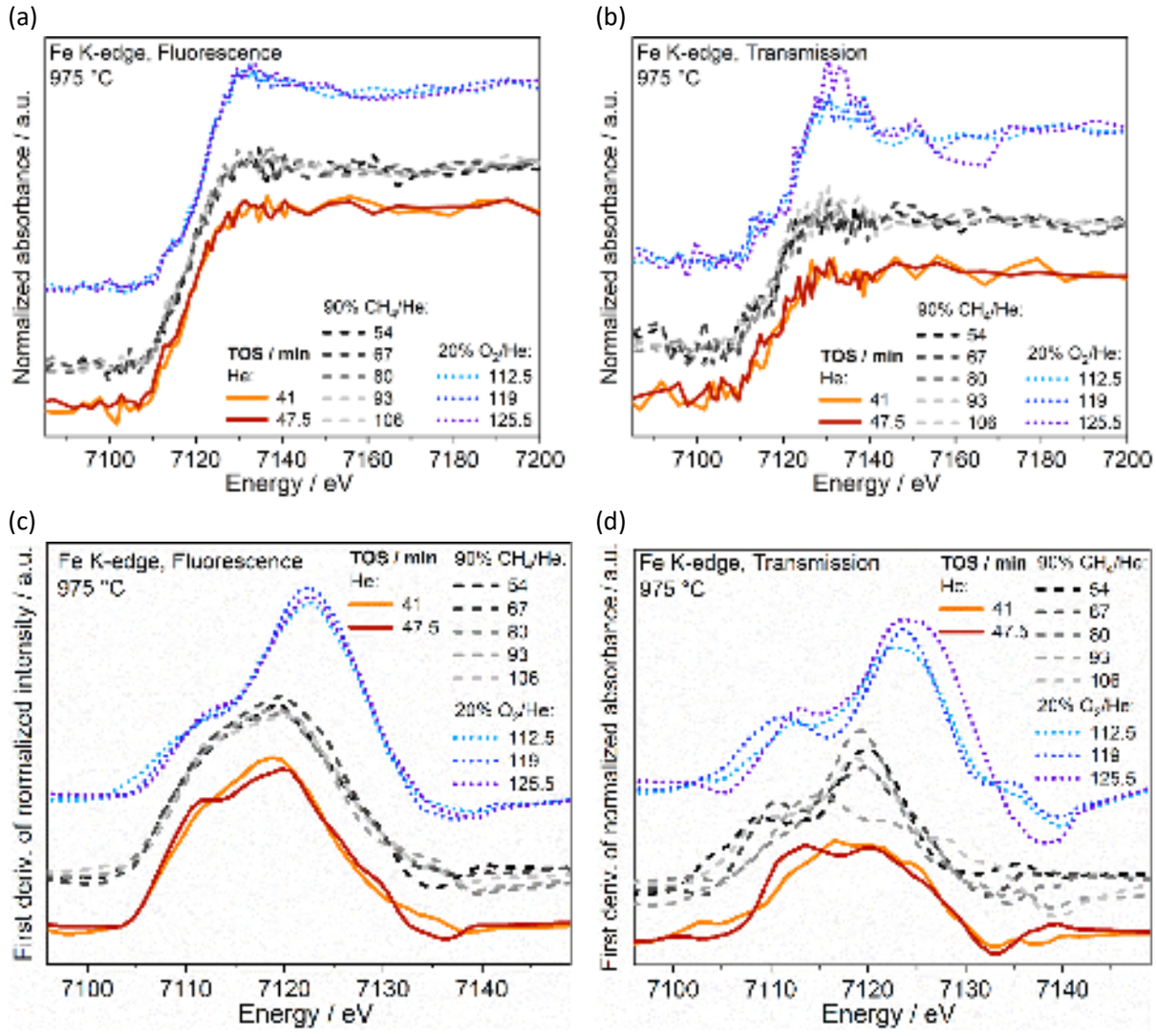

Fig. 8: (a, b) Normalized XANES spectra; (c, d) smoothed first derivative of XANES spectra at Fe K-edge of 0.5 % Fe/SiO_2 at 975 °C reaction temperature in He (━), 90% CH_4/He (- - -) and 20% O_2/He (· · ·) atmosphere recorded in (a, c) fluorescence and (b, d) transmission mode.

IV. CONCLUSION

A capillary plug flow microreactor embedded in a wire heating system has been presented to conduct *operando* measurements at temperatures of up to 1050 °C. An efficient heating system results in a homogeneous temperature profile along the catalyst bed and sufficient pre-heating of the reactant gas. The advanced cell allows fast change of reaction temperatures with high heating/cooling rates (100 °C/min). Due to its relatively small size, the setup fits to the majority of synchrotron beamlines. The catalytic activity can be monitored by measuring product gas composition with MS (used in the present

study for conversion of methane to ethylene and aromatics), FTIR (used to study the performance of the TWC catalyst) or gas chromatography. Avoiding iron in the setup and sufficiently shielding iron containing parts minimized interfering X-ray fluorescence signals from surrounding iron and thereby allowed measurement of catalysts with iron loading below 0.5 wt.%. We verified this by comparing X-ray absorption spectra collected in transmission and fluorescence measurement mode for a 0.5 % Fe/SiO_2 catalyst during direct conversion of methane under reaction conditions at 975 °C. Moreover, it was possible to measure Fe fluorescence of a 0.04 % Fe/SiO_2 sample with 90 % of the fluorescence signal originating from the sample. On the other hand, the reaction cell was successfully tested in *operando* XAS studies during the operation of a 2 % Pd/Al_2O_3 TWC at up to 800 °C for simultaneous removal of NO, CO and C_3H_6, which will allow us to derive structure-activity correlations. The good quality of the XAS data obtained for such high X-ray absorbing elements combined with the broad temperature window covered by this microreactor cell are essential parameters for understanding the functionality and also the deactivation behavior of TWC, which partly occurs at > 1000 °C and are hardly accessible with present *operando* cell designs. Hence, the application of the cell might pave new possibilities for understanding the structure and mechanism of further catalysts during high temperature reactions like oxidative coupling of methane, dry and steam reforming, aromatization and emission control. Moreover, the special design of the *operando* microreactor permits the study of processes conducted at elevated pressures and the combination of complementary characterization techniques such as XRD and Raman spectroscopy, further extending its applicability.

SUPPLEMENTARY MATERIAL

See supplementary material for Energy-dispersive X-ray spectroscopy (EDX) and X-ray fluorescence measurements (XRF) measurements of the Cu-ETP (CW004A) material and Kanthal® A-1 heating wire, additional XANES spectra of 0.04 % Fe/SiO_2-imp to evaluate the degree of background signals for X-ray fluorescence of surrounding iron and *operando* XANES measurements of the 0.5 % Fe/SiO_2 sample during heating up in He to 975 °C reaction temperature.

ACKNOWLEDGEMENTS

This work was supported by the German Research Foundation (Deutsche Forschungsgemeinschaft, DFG) through grant GR 3987/9-1 (in kind cooperation with Xiulian Pan (Dalian Institute of Chemical Physics, China) and through project CRC1441 (project number 426888090). Portions of this research were carried out at the light source PETRA III at DESY, a member of the Helmholtz Association (HGF). We would like to thank Edmund Welter and Ruidy Nemausat for assistance in using beamline P65. The authors thank Nilsu Öceş (ITCP/KIT) for preparing technical drawings, Michael Zimmermann (IKFT/KIT) for EDX measurements and the Institute for Beam Physics and Technology (IBPT/KIT) for the operation of the storage ring in the Karlsruhe Research Accelerator (KARA). Furthermore, the authors thank Kanthal GmbH Germany for providing resistive heating wires and Vasyl Marchuk (ITCP/KIT) for beamtime support. Florian Perrin (ESRF) is acknowledged for his technical help at the early stages of the reactor design and Dr. Thomas Bergfeldt (IAM-AWP/KIT) for ICP-OES measurements.

AIP PUBLISHING DATA SHARING POLICY

The data that support the findings of this study are available within the article and its supplementary material.

References

1 G. Ertl, H. Knözinger, J. Weitkamp, *Handbook of Heterogeneous Catalysis*. (John Wiley & Sons, 1997).
2 J. M. Thomas, W. J. Thomas, *Principles and practice of heterogeneous catalysis*. (John Wiley & Sons, 2014).
3 D. Macquarrie, Appl. Organomet. Chem. **19** (5), 696-696 (2005).
4 J.-D. Grunwaldt, J. B. Wagner, R. E. Dunin‐Borkowski, ChemCatChem **5** (1), 62-80 (2013).
5 J. K. Nørskov, F. Studt, F. Abild-Pedersen, T. Bligaard, *Fundamental concepts in heterogeneous catalysis*. (John Wiley & Sons, 2014).
6 B. M. Weckhuysen, Phys. Chem. Chem. Phys. **5** (20), 4351-4360 (2003).
7 K. F. Kalz, I. R. Kraehnert, P. Muslim Dvoyashkin, I. R. Dittmeyer, R. Gläser, I. U. Krewer, K. Reuter, J.-D. Grunwaldt, ChemCatChem **9** (1), 17 (2017).
8 B. R. Fingland, F. H. Ribeiro, J. T. Miller, Catal. Lett. **131** (1), 1-6 (2009).
9 J.-D. Grunwaldt, B. S. Clausen, Top. Catal. **18** (1-2), 37-43 (2002).
10 S. R. Bare, T. Ressler, Adv. Catal. **52**, 339-465 (2009).
11 S. Bordiga, E. Groppo, G. Agostini, J. A. van Bokhoven, C. Lamberti, Chem. Rev. **113** (3), 1736-1850 (2013).
12 D. E. Doronkin, H. Lichtenberg, J.-D. Grunwaldt, *Cell designs for in situ and operando studies.* In: "*XAFS Techniques for Catalysts, Nanomaterials, and Surfaces" (eds. Y. Iwasawa, K. Asakura, M. Tada)*, Springer, **2017**, pp. 75-89.
13 A. M. Gänzler, M. Casapu, P. Vernoux, S. Loridant, F. J. Cadete Santos Aires, T. Epicier, B. Betz, R. Hoyer, J. D. Grunwaldt, Angew. Chem. Int. Ed. **56** (42), 13078-13082 (2017).
14 D. Vantelon, P. Lagarde, A. M. Flank, E. Berrier, X. Secordel, S. Cristol, C. L. Fontaine, F. Villain, V. Briois, Phase Transit. **82** (4), 322-335 (2009).
15 P. Sprenger, M. Stehle, A. Gaur, A. M. Gänzler, D. Gashnikova, W. Kleist, J.-D. Grunwaldt, ACS Catal. **8** (7), 6462-6475 (2018).
16 R. Dalla Betta, M. Boudart, K. Foger, D. Löffler, J. Sanchez‐Arrieta, Rev. Sci. Instrum. **55** (12), 1910-1913 (1984).
17 F. Kampers, T. Maas, J. Van Grondelle, P. Brinkgreve, D. Koningsberger, Rev. Sci. Instrum. **60** (8), 2635-2638 (1989).
18 G. Meitzner, S. R. Bare, D. Parker, H. Woo, D. A. Fischer, Rev. Sci. Instrum. **69** (7), 2618-2621 (1998).
19 P. Riello, A. Lausi, J. Macleod, J. R. Plaisier, G. Zerauschek, P. Fornasiero, J. Synchrotron Rad. **20** (1), 194-196 (2013).
20 H. Huwe, M. Fröba, J. Synchrotron Rad. **11** (4), 363-365 (2004).
21 L. Nguyen, Y. Tang, Y. Li, X. Zhang, D. Wang, F. Tao, Rev. Sci. Instrum. **89** (5), 054103 (2018).
22 G. Guilera, B. Gorges, S. Pascarelli, H. Vitoux, M. A. Newton, C. Prestipino, Y. Nagai, N. Hara, J. Synchrotron Rad. **16** (5), 628-634 (2009).
23 J.-D. Grunwaldt, M. Caravati, S. Hannemann, A. Baiker, Phys. Chem. Chem. Phys. **6** (11), 3037-3047 (2004).

24 B. Clausen, G. Steffensen, B. Fabius, J. Villadsen, R. Feidenhans, H. Topsøe, J. Catal. **132** (2), 524-535 (1991).
25 G. Sankar, J. M. Thomas, F. Rey, G. N. Greaves, J. Chem. Soc., Chem. Commun. (24), 2549-2550 (1995).
26 J.-D. Grunwaldt, N. van Vegten, A. Baiker, W. van Beek, in *J. Phys. Conf. Ser., Vol. 190*, IOP Publishing, **2009**, p. 012160.
27 A. Aguilar-Tapia, S. Ould-Chikh, E. Lahera, A. Prat, W. Delnet, O. Proux, I. Kieffer, J.-M. Basset, K. Takanabe, J.-L. Hazemann, Rev. Sci. Instrum. **89** (3), 035109 (2018).
28 P. J. Chupas, K. W. Chapman, C. Kurtz, J. C. Hanson, P. L. Lee, C. P. Grey, J. Appl. Crystallogr. **41** (4), 822-824 (2008).
29 S. J. Figueroa, D. Gibson, T. Mairs, S. Pasternak, M. A. Newton, M. Di Michiel, J. Andrieux, K. C. Christoforidis, A. Iglesias-Juez, M. Fernández-García, J. Appl. Crystallogr. **46** (5), 1523-1527 (2013).
30 J. Andrieux, C. Chabert, A. Mauro, H. Vitoux, B. Gorges, T. Buslaps, V. Honkimaeki, J. Appl. Crystallogr. **47** (1), 245-255 (2014).
31 X. Guo, G. Fang, G. Li, H. Ma, H. Fan, L. Yu, C. Ma, X. Wu, D. Deng, M. Wei, D. Tan, R. Si, S. Zhang, J. Li, L. Sun, Z. Tang, X. Pan, X. Bao, Science **344** (6184), 616-619 (2014).
32 S. J. Han, S. Lee, H. W. Kim, S. K. Kim, Y. T. Kim, ACS Catal. **9**, 7984-7997 (2019).
33 S. C. Oh, E. Schulman, J. Zhang, J. Fan, Y. Pan, J. Meng, D. Liu, Angew. Chem. (2019).
34 S. Sahoo, A. C. Reber, S. N. Khanna, Chem. Phys. Lett. **660**, 48-54 (2016).
35 P. Šot, M. A. Newton, D. Baabe, M. D. Walter, A. P. van Bavel, A. D. Horton, C. Copéret, J. A. van Bokhoven, Chem. Eur. J. (2020).
36 R. M. Heck, R. J. Farrauto, Appl. Catal. A **221** (1-2), 443-457 (2001).
37 A. M. Gänzler, M. Casapu, F. Maurer, H. Störmer, D. Gerthsen, G. Ferré, P. Vernoux, B. Bornmann, R. Frahm, V. Murzin, ACS Catal. **8** (6), 4800-4811 (2018).
38 J. J.-g. Hsia, *Experimental Investigation on the Reflectivity of Al, Cu, Zn and Ni and Its Comparison with Theory*, Purdue University **1968**.
39 Ľ. Straka, S. Hašová, Int. J. Adv. Manuf. Technol. **97** (5-8), 2647-2654 (2018).
40 E. Welter, R. Chernikov, M. Herrmann, R. Nemausat, in *AIP Conf. Proc., Vol. 2054*, AIP Publishing LLC, **2019**, p. 040002.
41 A. Zimina, K. Dardenne, M. Denecke, D. Doronkin, E. Huttel, H. Lichtenberg, S. Mangold, T. Pruessmann, J. Rothe, T. Spangenberg, R. Steininger, T. Vitova, H. Geckeis, J.-D. Grunwaldt, Rev. Sci. Instrum. **88** (11), 113113 (2017).
42 N. E. Tsakoumis, A. Voronov, M. Rønning, W. van Beek, Ø. Borg, E. Rytter, A. Holmen, J. Catal. **291**, 138-148 (2012).
43 M. Gentzen, D. E. Doronkin, T. L. Sheppard, A. Zimina, H. Li, J. Jelic, F. Studt, J.-D. Grunwaldt, J. Sauer, S. Behrens, Angew. Chem. Int. Ed. **58** (44), 15655-15659 (2019).
44 A. M. Gänzler, M. Casapu, A. Boubnov, O. Müller, S. Conrad, H. Lichtenberg, R. Frahm, J.-D. Grunwaldt, J. Catal. **328**, 216-224 (2015).
45 S. Müller, A. Zimina, R. Steininger, S. Flessau, J. Osswald, J.-D. Grunwaldt, ACS Sens. **5** (8), 2486-2496 (2020).
46 D. R. Lide, *CRC Handbook of Chemistry and Physics*. (CRC press, 2004).
47 D. Soulivong, S. Norsic, M. Taoufik, C. Coperet, J. Thivolle-Cazat, S. Chakka, J.-M. Basset, J. Am. Chem. Soc. **130** (15), 5044-5045 (2008).
48 B. Ravel, M. Newville, J. Synchrotron Rad. **12** (4), 537-541 (2005).
49 P. Lott, M. Eck, D. E. Doronkin, R. Popescu, M. Casapu, J.-D. Grunwaldt, O. Deutschmann, Top. Catal. **62** (1-4), 164-171 (2019).
50 M. Høj, K. Linde, T. K. Hansen, M. Brorson, A. D. Jensen, J.-D. Grunwaldt, Appl. Catal. A **397** (1-2), 201-208 (2011).

51 J. Wang, H. Chen, Z. Hu, M. Yao, Y. Li, Cat. Rev. Sci. Eng. **57** (1), 79-144 (2015).
52 D. Chatterjee, O. Deutschmann, J. Warnatz, Faraday Discuss. **119**, 371-384 (2002).
53 Y. Lu, M. S. Kumar, G. L. Chiarello, P. D. Eggenschwiler, C. Bach, M. Weilenmann, A. Spiteri, A. Weidenkaff, D. Ferri, Catal. Commun. **39**, 55-59 (2013).
54 M. Fernández-Garcıa, A. Iglesias-Juez, A. Martınez-Arias, A. Hungrıa, J. Anderson, J. Conesa, J. Soria, J. Catal. **221** (2), 594-600 (2004).
55 E. Ogel, M. Casapu, D. Doronkin, R. Popescu, H. Stormer, C. Mechler, G. Marzun, S. Barcikowski, M. Turk, J.-D. Grunwaldt, J. Phys. Chem. C **123** (9), 5433-5446 (2019).
56 A. Boubnov, S. Dahl, E. Johnson, A. P. Molina, S. B. Simonsen, F. M. Cano, S. Helveg, L. J. Lemus-Yegres, J.-D. Grunwaldt, Appl. Catal. B **126**, 315-325 (2012).
57 P. Schwach, X. Pan, X. Bao, Chem. Rev. **117** (13), 8497-8520 (2017).
58 D. Klukowski, P. Balle, B. Geiger, S. Wagloehner, S. Kureti, B. Kimmerle, A. Baiker, J.-D. Grunwaldt, Appl. Catal. B **93** (1-2), 185-193 (2009).
59 M. Høj, M. J. Beier, J.-D. Grunwaldt, S. Dahl, Appl. Catal. B **93** (1-2), 166-176 (2009).

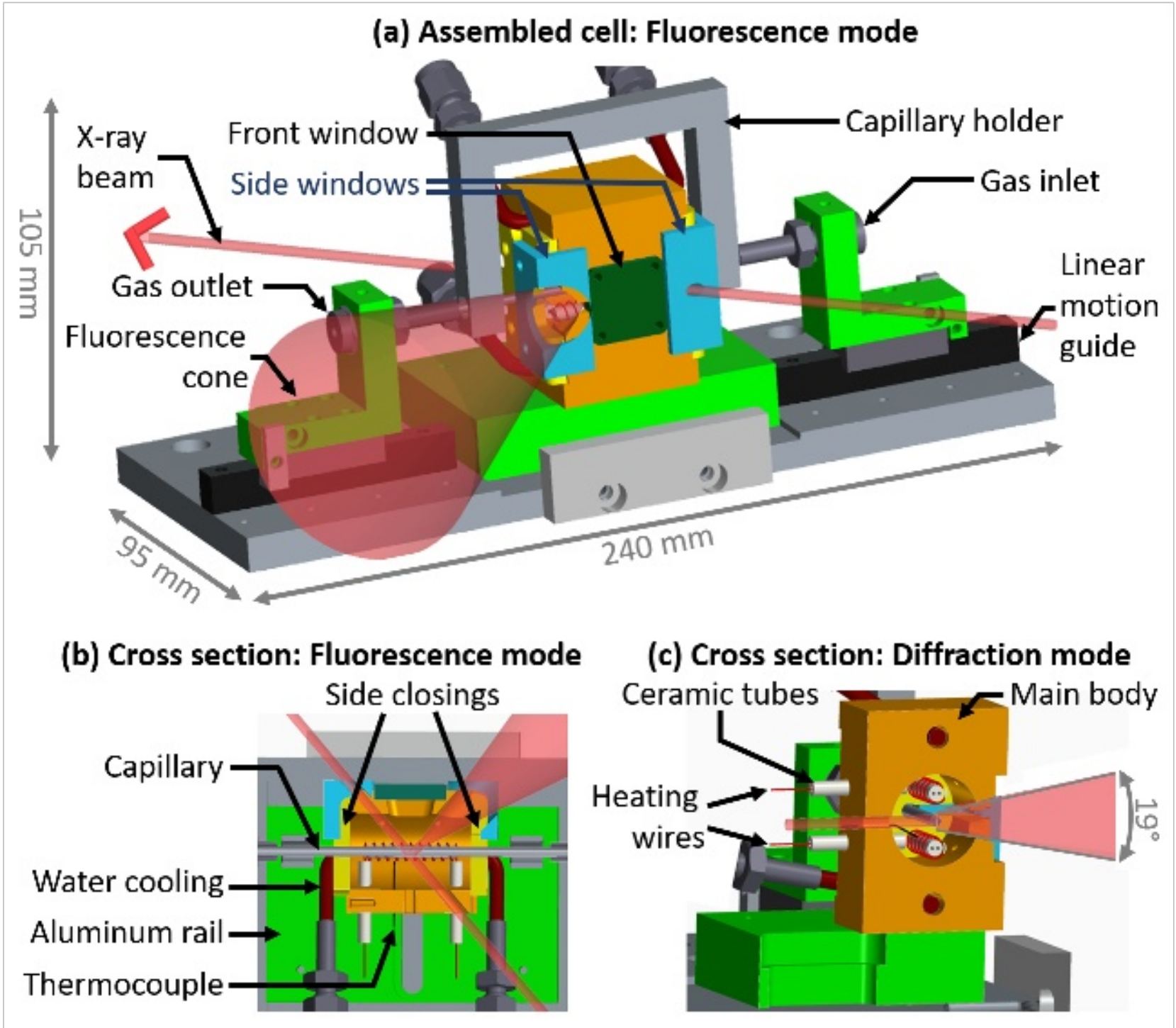
(a) Assembled cell: Fluorescence mode
X-ray beam
Front window
Capillary holder
Side windows
Gas inlet
105 mm
Gas outlet
Linear motion guide
Fluorescence cone
95 mm
240 mm
(b) Cross section: Fluorescence mode
Side closings
Capillary
Water cooling
Aluminum rail
Thermocouple
(c) Cross section: Diffraction mode
Ceramic tubes
Main body
Heating wires
19°

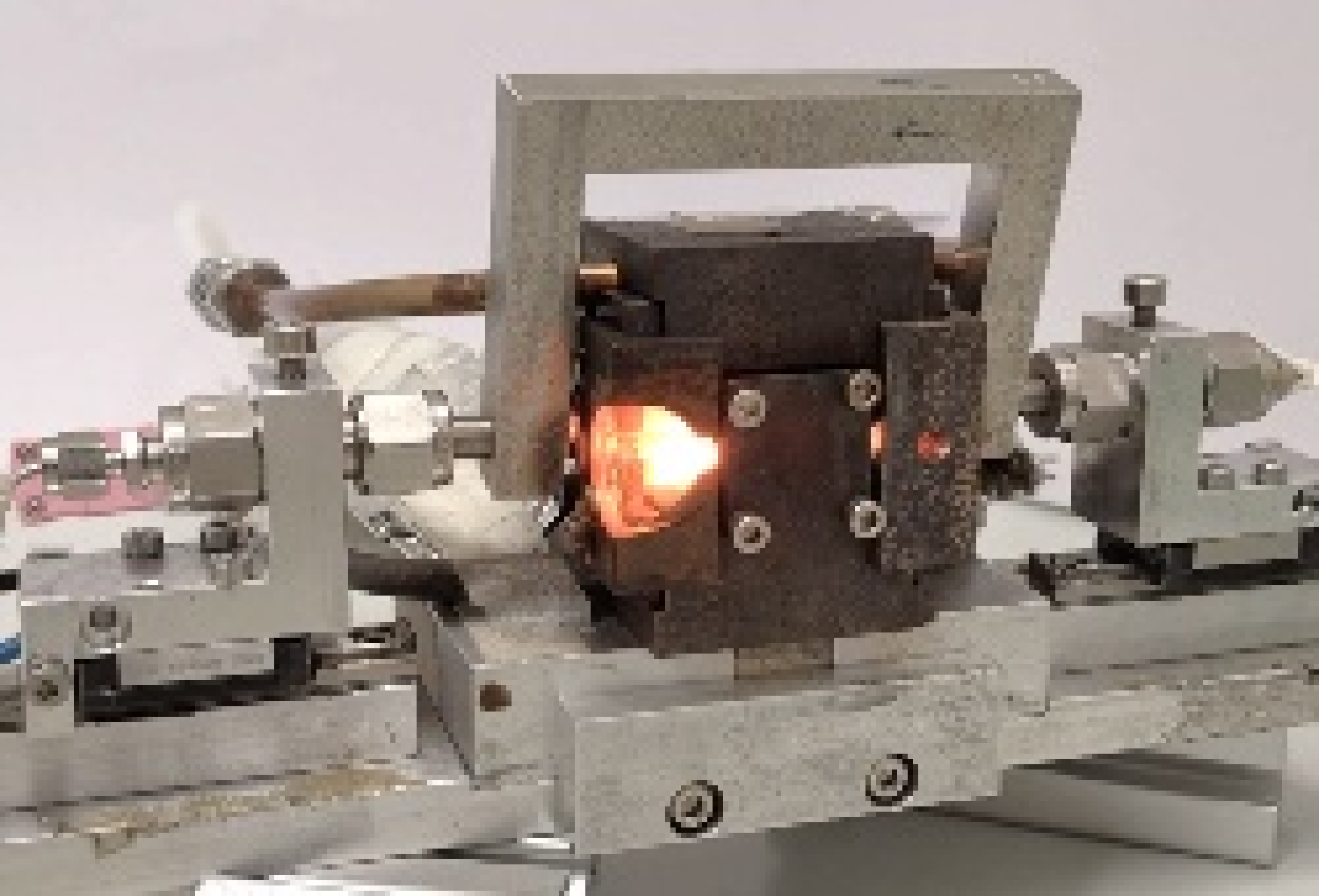

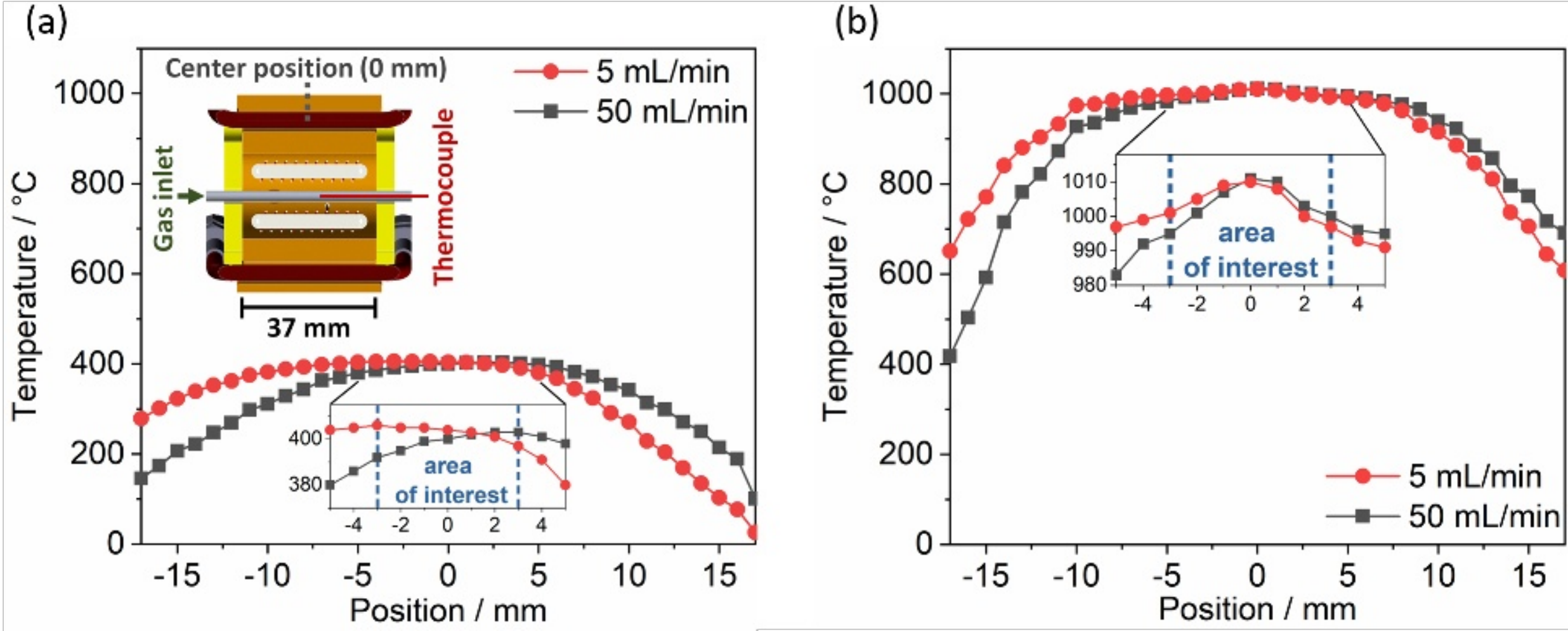
(a)
Center position (0 mm)
5 mL/min
50 mL/min
Gas inlet
Thermocouple
37 mm
Temperature / °C
Position / mm
area
of interest
(b)
5 mL/min
50 mL/min
Temperature / °C
Position / mm
area
of interest

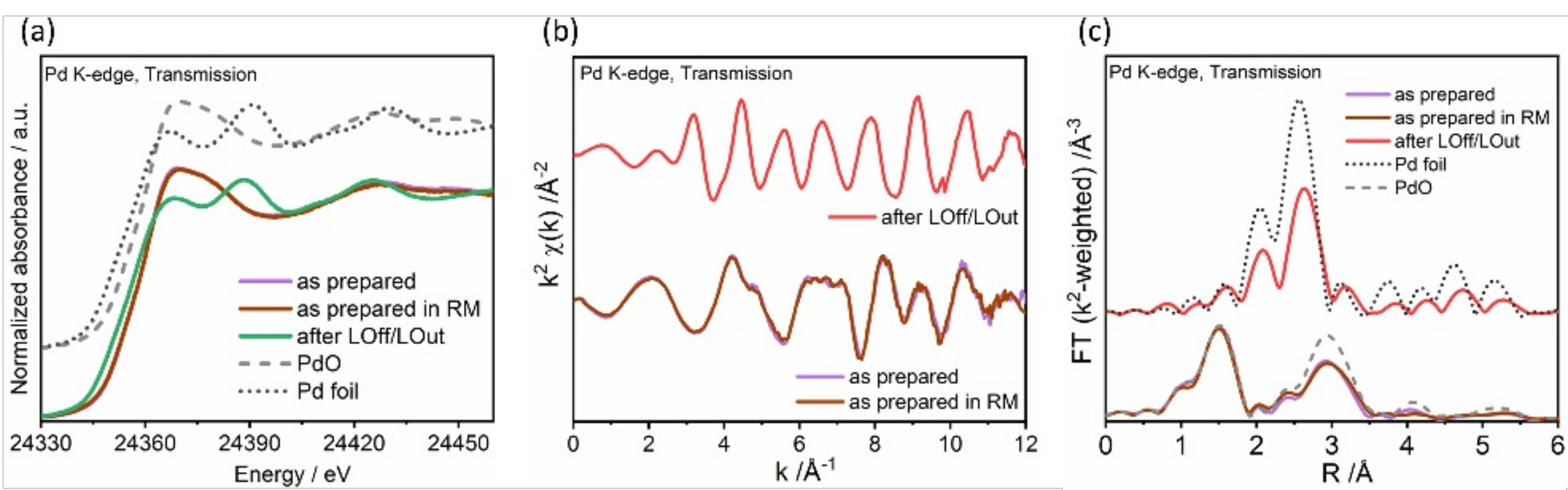
(a)
Pd K-edge, Transmission
Normalized absorbance / a.u.
as prepared
as prepared in RM
after LOff/LOut
PdO
Pd foil
24330
24360
24390
24420
24450
Energy / eV
(b)
Pd K-edge, Transmission
k² χ(k) /Å⁻²
after LOff/LOut
as prepared
as prepared in RM
0
2
4
6
8
10
12
k /Å⁻¹
(c)
Pd K-edge, Transmission
as prepared
as prepared in RM
after LOff/LOut
Pd foil
PdO
FT (k²-weighted) /Å⁻³
0
1
2
3
4
5
6
R /Å

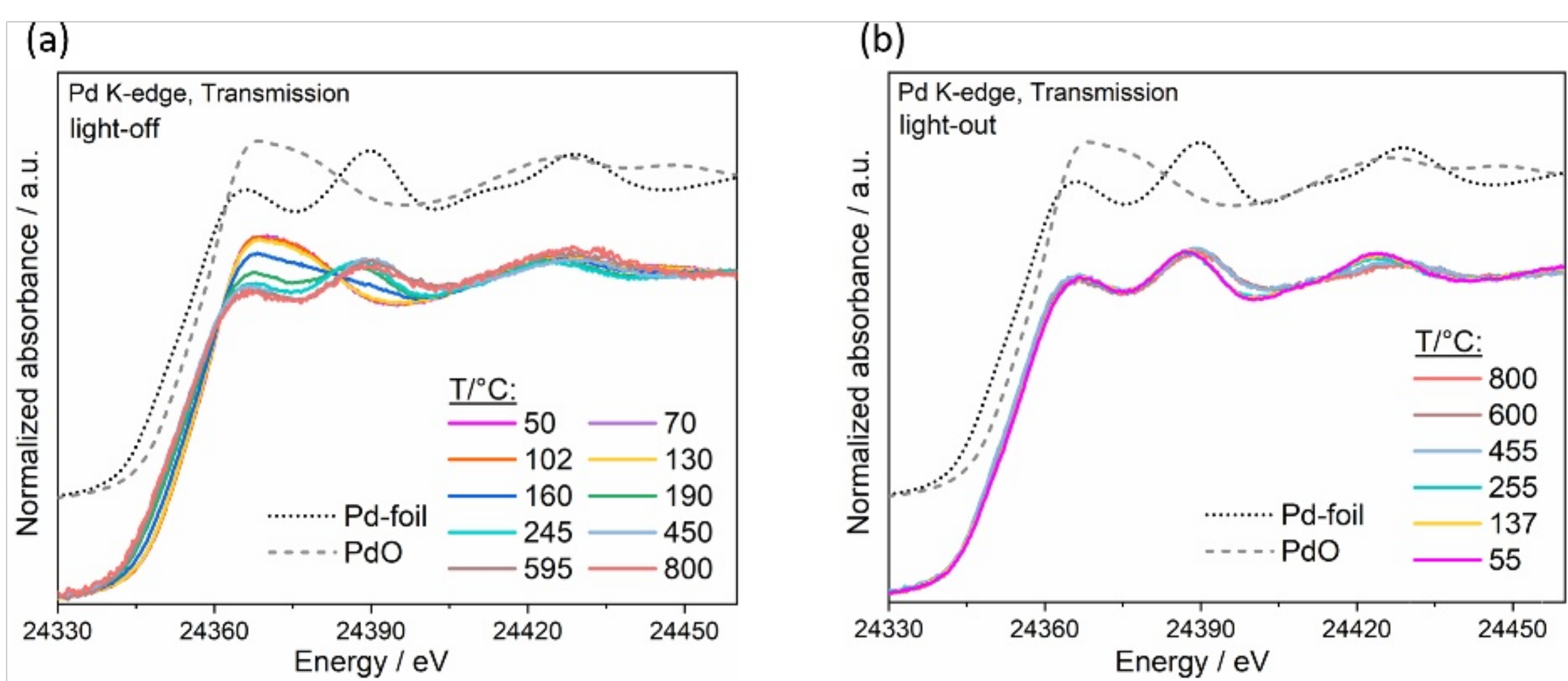
(a)
Pd K-edge, Transmission
light-off
Normalized absorbance / a.u.
T/°C:
50
70
102
130
160
190
245
450
595
800
Pd-foil
PdO
24330
24360
24390
24420
24450
Energy / eV
(b)
Pd K-edge, Transmission
light-out
Normalized absorbance / a.u.
T/°C:
800
600
455
255
137
55
Pd-foil
PdO
24330
24360
24390
24420
24450
Energy / eV

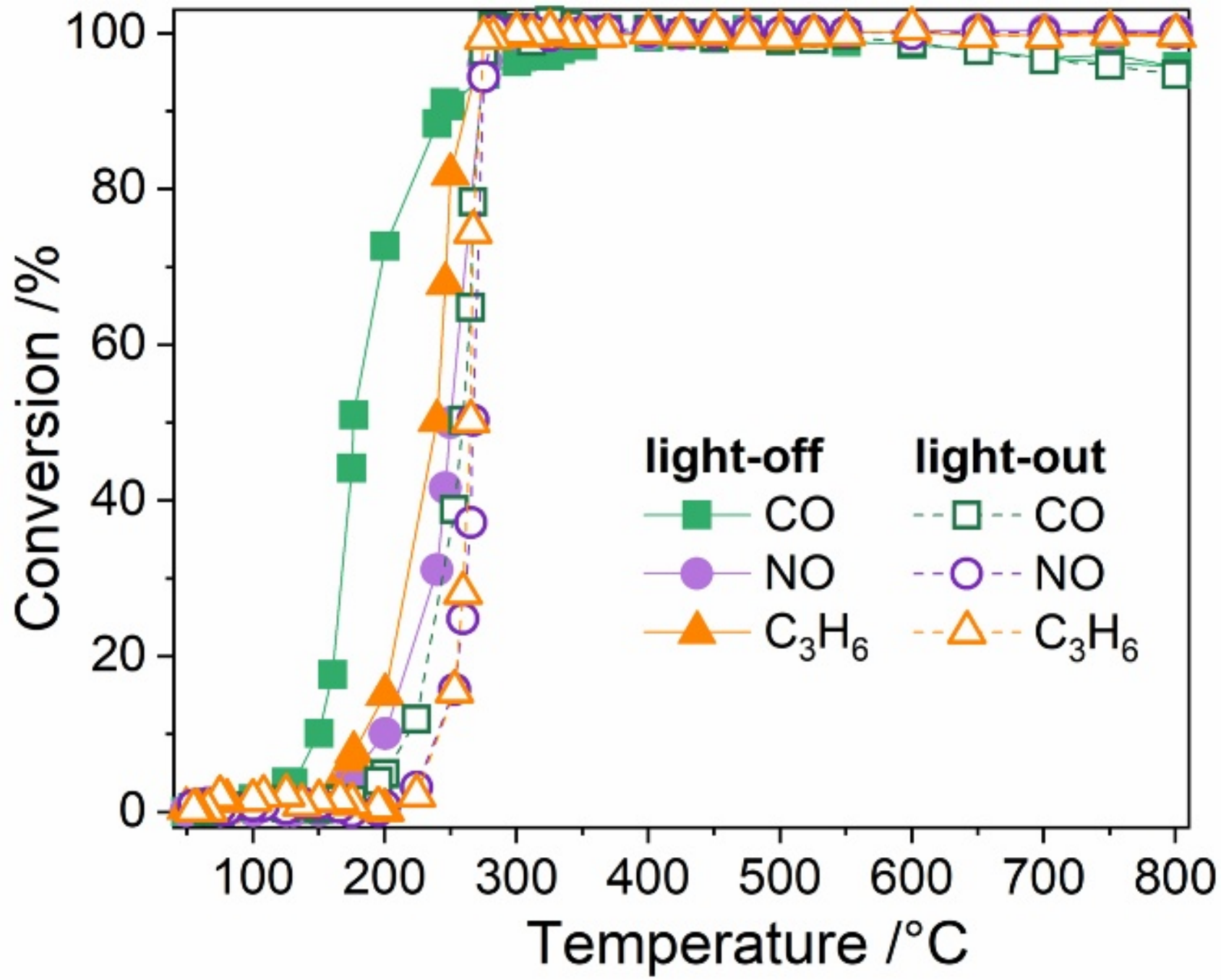
Conversion /%
Temperature /°C
0
20
40
60
80
100
100
200
300
400
500
600
700
800
light-off
light-out
CO
NO
C3H6
CO
NO
C3H6

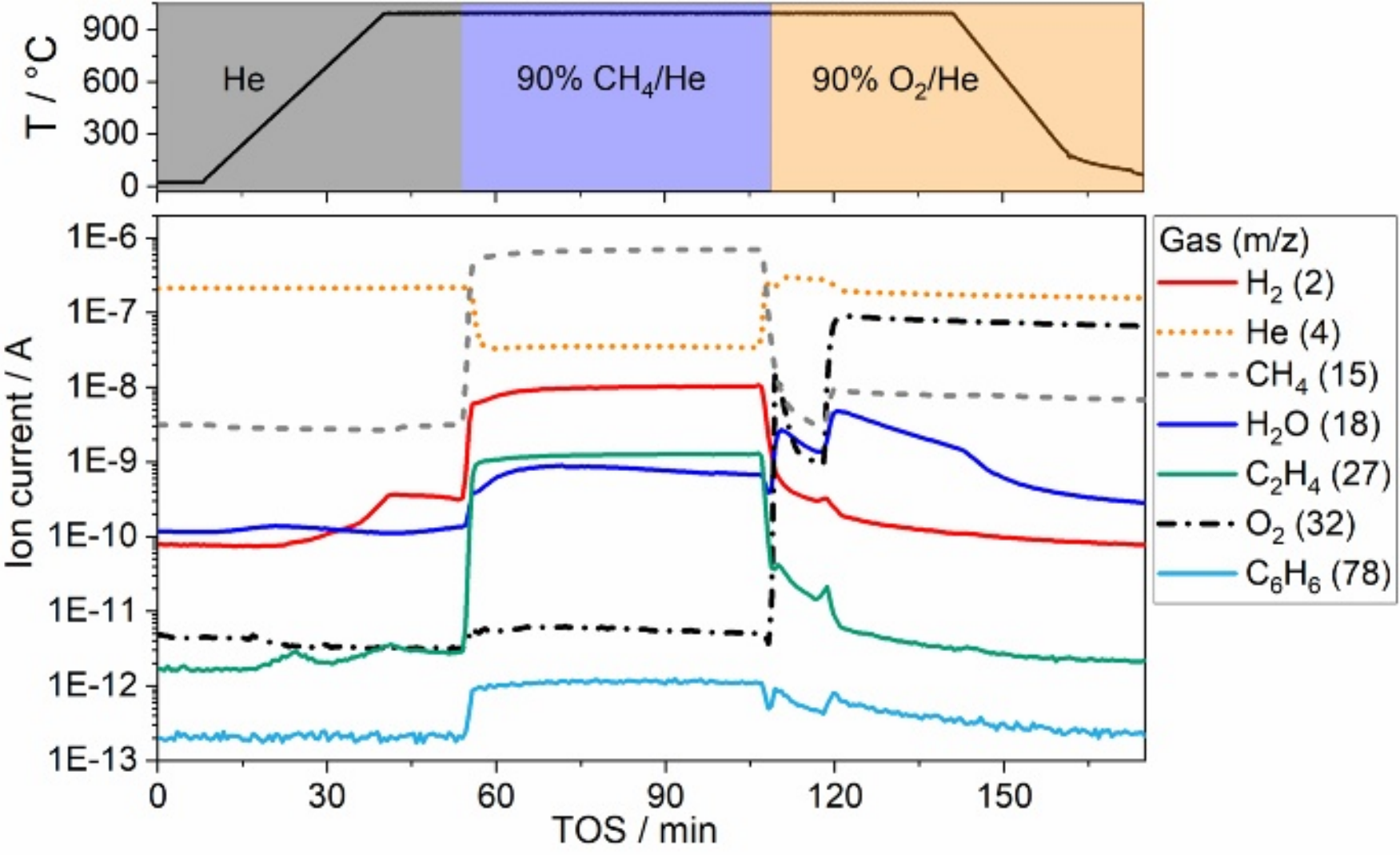
T / °C
900
600
300
0
He
90% CH4/He
90% O2/He
Ion current / A
1E-6
1E-7
1E-8
1E-9
1E-10
1E-11
1E-12
1E-13
0
30
60
90
120
150
TOS / min
Gas (m/z)
H2 (2)
He (4)
CH4 (15)
H2O (18)
C2H4 (27)
O2 (32)
C6H6 (78)

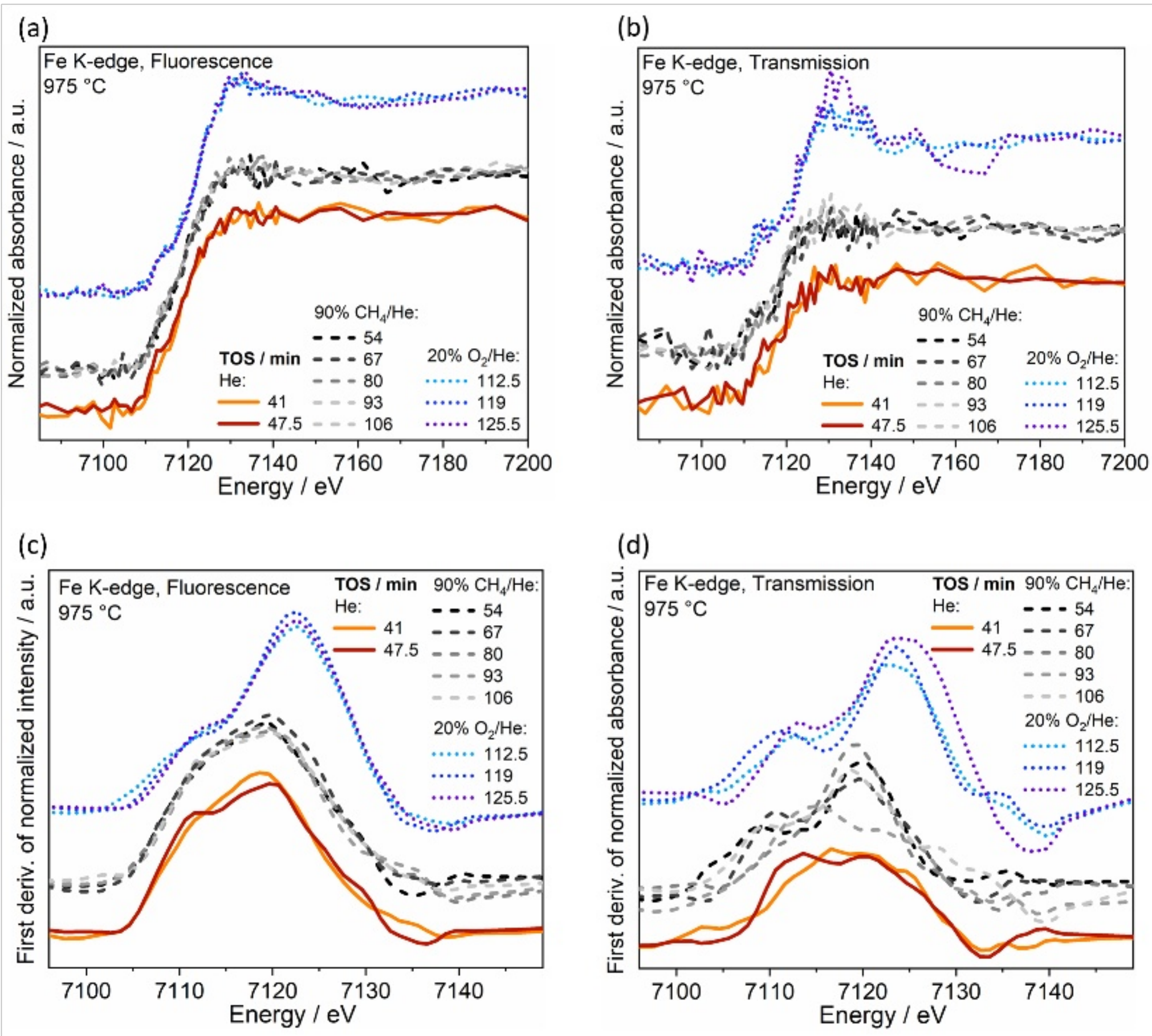
(a)
Fe K-edge, Fluorescence
975 °C
Normalized absorbance / a.u.
Energy / eV
7100
7120
7140
7160
7180
7200
TOS / min
He:
41
47.5
90% CH4/He:
54
67
80
93
106
20% O2/He:
112.5
119
125.5
(b)
Fe K-edge, Transmission
975 °C
Normalized absorbance / a.u.
Energy / eV
(c)
Fe K-edge, Fluorescence
975 °C
First deriv. of normalized intensity / a.u.
Energy / eV
7100
7110
7120
7130
7140
(d)
Fe K-edge, Transmission
975 °C
First deriv. of normalized absorbance / a.u.
Energy / eV